

Evolution of Submesoscale Cyclones on the Batumi Anticyclone Periphery Based on the Numerical Simulation Data

A. A. Bogdanov ✉, A. I. Mizyuk, A. A. Kubryakov

Marine Hydrophysical Institute of RAS, Sevastopol, Russian Federation

✉ artem96.96@bk.ru

Abstract

Purpose. The paper is purposed at studying the characteristics and evolution of submesoscale cyclonic eddies attached to the Batumi anticyclone.

Methods and Results. The results of numerical simulation based on the NEMO model data for 2008–2009 and on the algorithm for automatic eddy identification, permitted to obtain the data on evolution of the dynamic and thermohaline structure of such eddies, and the reasons for their formation and dissipation. When in 2008 the Batumi anticyclone was passing, seven pronounced stable submesoscale rounded cyclonic eddies were detected on its periphery. The lifetime of some eddies achieves 20 days, vorticity anomalies in them can reach the 200 m depth, and vertical velocities can exceed 10 m/day.

Conclusions. The submesoscale cyclonic eddies are formed at intensification of the Batumi anticyclone and at its displacement to the west towards Cape Fener. Increase of velocity shear arising during interaction of the Batumi anticyclone with the cape, results in formation of the cyclonic vorticity area which in some cases transforms into a submesoscale cyclonic eddy. Further, such eddies separate from the coast and move along the Batumi anticyclone periphery in the anticyclonic direction. The highest energy of submesoscale cyclonic eddies is observed at the moment of their formation, and then follows their slow dissipation, that is related to the process of their elongation due to the velocity shear at the Batumi anticyclone periphery. This process gradually intensifies with weakening of a cyclonic vortex and results in its transformation into a vortex filament.

Keywords: Black Sea, numerical modeling, NEMO, Batumi anticyclone, submesoscale cyclonic eddies, eddy, anticyclone

Acknowledgments: The evolution and dissipation processes of submesoscale cyclones were studied with the support by the Russian Science Foundation grant 21-77-10052. The eddies were identified at the support of the state assignment of MHI RAS on theme FNNN-2021-0003. Data processing was supported by state assignment of MHI RAS on theme FNNN-2021-0007.

For citation: Bogdanov, A.A., Mizyuk, A.I. and Kubryakov, A.A., 2022. Evolution of Submesoscale Cyclones on the Batumi Anticyclone Periphery Based on the Numerical Simulation Data. *Physical Oceanography*, 29(6), pp. 550-566. doi:10.22449/1573-160X-2022-6-550-566

DOI: 10.22449/1573-160X-2022-6-550-566

© A. A. Bogdanov, A. I. Mizyuk, A. A. Kubryakov, 2022

© Physical Oceanography, 2022

1. Introduction

Submesoscale cyclones have a significant local effect on the horizontal and vertical exchange, mixing and water stratification [1–3], transport of suspended matter in the coastal zone [4–6], nutrient fluxes and biological processes in the marine environment [6–8]. Submesoscale processes in the Black Sea are characterized by pronounced seasonal and spatial variability [4, 6, 9]. One of the generation areas of submesoscale cyclonic eddies (SCE) in the Black Sea is the periphery of mesoscale anticyclones [6, 10, 11]. Sharp velocity shear and vorticity gradients at the boundary of these eddies, especially in the coastal zone in the presence of capes [6], cause the appearance of local zones of rise and divergence of water [10, 12, 13]. Such processes, in particular, were noted in the southeastern part



of the sea [11], where the Batumi anticyclone (BA) is located, one of the most intense eddy formations in the Black Sea [13]. The BA is the most stationary eddy formation [14, 15]; it interacts with the coastline for a long time period, which contributes to the SCE formation. Examples in Fig. 1 demonstrate the formation of several such eddies at the quasi-stationary BA boundary. SCEs significantly affect the distribution of coastal turbid waters and are often characterized by a brightness maximum in their core, which indicates their ability to transport suspended matter (for more detail, see [4]).

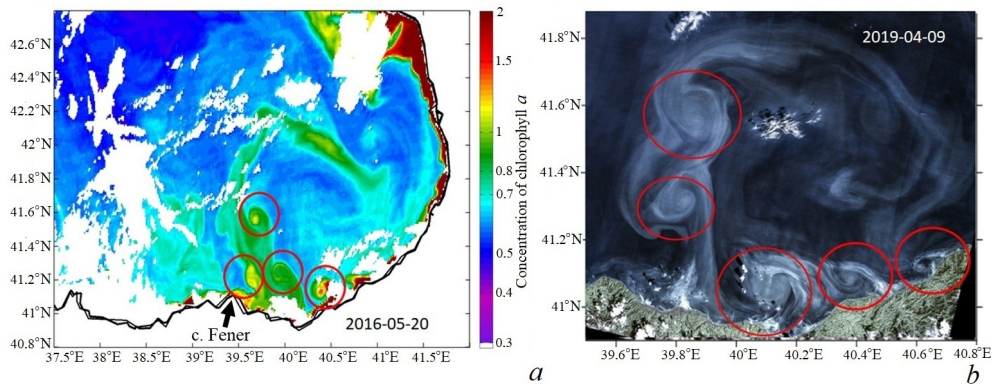


Fig. 1. Submesoscale cyclones (red ovals) at the BA periphery based on the MODIS measurements for May 20, 2016 (*a*); and based on the Sentinel-2 data for April 9, 2019 (*b*)

Despite the fact that the process of SCE formation at the periphery of anticyclones was studied in detail in idealistic models in a number of recent papers [13, 16], studies of the evolution of attached SCEs based on realistic numerical simulations have hardly been carried out previously.

Development of high-resolution numerical models, as well as the appearance of automatic eddy identification methods, provide detailed information on the evolution of the dynamic and thermohaline characteristics of submesoscale cyclones. The present paper is aimed at studying the features of generation, development and SCE dissipation at the BA periphery based on the results of realistic numerical modeling with high spatial resolution using algorithms for automatic eddy identification.

2. Data and methods

2.1. Numerical modeling

To study the evolution of eddy structures, the present work uses the results of calculations based on the NEMO complex for numerical modeling of the circulation for 2008–2009 [17]. The hydrodynamic block is based on a system of primitive hydrodynamic equations. For nonlinear terms in the equations of heat and salt transfer – diffusion, the TVD scheme is used. Discretization in time is carried out by means of a modified "leapfrog" scheme. Vertically, a z -coordinate with a fractional step is used. The UNESCO formula is used as the state equation. The vertical turbulent mixing parametrization is carried out using the $k - \epsilon$ model. To describe the lateral exchange, a standard biharmonic operator with negative viscosity and

diffusion coefficients, modulo equal to $4 \cdot 10^7 \text{ m}^4/\text{s}$ and $8 \cdot 10^6 \text{ m}^4/\text{s}$, respectively, is used.

The computational domain covers the Black, Azov and Marmara seas and is presented as a quasi-regular grid with a spatial resolution of $1/96^\circ$ in latitude and $1/69^\circ$ in longitude. This corresponds to a step of $\sim 1.157 \text{ km}$ along the meridian, the zonal step changes uniformly from 1100 m in the north to 1230 m in the south. Temperature and salinity fields taken from the product base of the Black Sea Marine Forecast Center were used as initial conditions for the Black Sea ¹. Bottom topography was built on the basis of EMODnet project data with a resolution of $7.5'' \times 7.5''$, which is about 200 m in the meridional direction.

To initialize the model based on the results of model calculations of the FSBSI FRC MHI Marine Forecast Center system, the temperature and salinity fields were prepared for August 15, 2007.

For boundary conditions on the surface, downstream longwave and shortwave radiation fluxes, precipitation in liquid and solid phases, the horizontal component of wind speed at a height of 10 m and air temperature and humidity fields at a height of 2 m are used. This data was obtained from the global atmospheric reanalysis of the European Center for Medium-Range Weather Forecasts (ECMWF) of the latest ERA5 generation. Spatial resolution of the product fields is 0.25° , and the time discretization is 1 hour . The noted meteorological parameters with the initial time discreteness were used to calculate the total heat fluxes, mass and wind friction stress using the bulk formulas of the CORE protocol (Coordinated Ocean-ice Reference Experiments).

The model parameters and configuration features are presented in more detail in [18, 19]. Model fields with a time resolution of 1 day were used for the analysis. The southeastern part of the Black Sea with coordinates $38^\circ\text{--}42^\circ\text{E}$ and $41^\circ\text{--}43^\circ\text{N}$ was chosen for the study.

2.2. Automatic identification of eddies

The automatic identification of eddies in this work is based on the determination of the Okubo – Weiss (OW) parameter [20, 21]. The following algorithm was used:

Step 1. Value of the vertical component of the relative vorticity of the current (hereinafter referred to as vorticity) is calculated from the data on the velocity of currents at a horizon of 20 m :

$$\zeta = \frac{\partial v}{\partial x} - \frac{\partial u}{\partial y},$$

where v is y -axis velocity; u is x -axis velocity.

Step 2. For each cell, the OW parameter is calculated [20] by the following formula

$$W = S_n^2 + S_s^2 - \zeta^2,$$

¹ MyOcean. *MyOcean Service*. 2018. [online] Available at: <http://bsmfc.net> [Accessed: 25 November 2022].

where $S_n^2 = \frac{\partial u}{\partial x} - \frac{\partial v}{\partial y}$ is the normal stress component; $S_s^2 = \frac{\partial v}{\partial x} + \frac{\partial u}{\partial y}$ is the shear stress component.

Step 3. A negative value of the OW parameter indicates that the relative rotation of the particles dominates in the fluid, and vice versa, when it is positive, shear and normal stress dominate. In this case, the OW parameter is negative for both cyclones and anticyclones [21]. Therefore, to identify eddies, regions with the OW parameter value that is less than a certain limit are selected. In this paper, this limit was taken empirically equal to $W_{kr} = -2 \cdot 10^{-10} \text{ 1/s}^2$. A set of grid nodes with common boundaries that satisfies this condition is the eddy core. In the calculation, only eddies containing more than six cells, i.e., eddies with a core radius exceeding 2 km, were identified.

Step 4. For eddy tracking, all of them are identified on two maps of the OW parameters (at the given time step and the previous one): their centers and the number of cells that they consist of are marked. Further, with each eddy from the set of the previous time step, the following procedures are cyclically carried out:

- for the selected eddy (B1) on the first map, the coordinates of its center are determined. Depending on the maximum possible eddy speed in the given region and the time step, the maximum search area radius between the same eddy manifestations on two consecutive maps is selected. In the present paper, the value of 0.3 m/s with a time step of 24 h was chosen as the maximum moving velocity, which corresponds to a search radius of 29 km;
- further, from the eddies in the selected search area, the B2 eddy closest to B1 with the same vorticity sign is selected;
- B1 is excluded from the set of eddies of the previous time step, and B2 is excluded from the next time step map. If at any of the steps there is no subsequent eddy satisfying the conditions, then it is considered that B1 is the last reflection of the eddy trajectory – the eddy has dissipated.

3. Results

3.1. Statistics of identified eddies

Based on the algorithm described above, in the study area ($38^\circ\text{--}42^\circ\text{E}$ and $41^\circ\text{--}43^\circ\text{N}$) for 2008–2009 a total of 1975 cyclones with an average lifetime of 7 days and a maximum of 73 days and 1454 anticyclones with an average lifetime of 7 days and a maximum of 229 days were identified.

Fig. 2, *a* shows the statistical distribution of the radii of all vortex structures identified in 2008–2009. In agreement with previous works [16], many more small eddies (with a radius of less than 5 km) than the large ones are observed. Let us note that the Okubo–Weiss method used in this work permits to identify only the core of eddies. The real size of the eddy-influenced area can be 1.5–2 times larger.

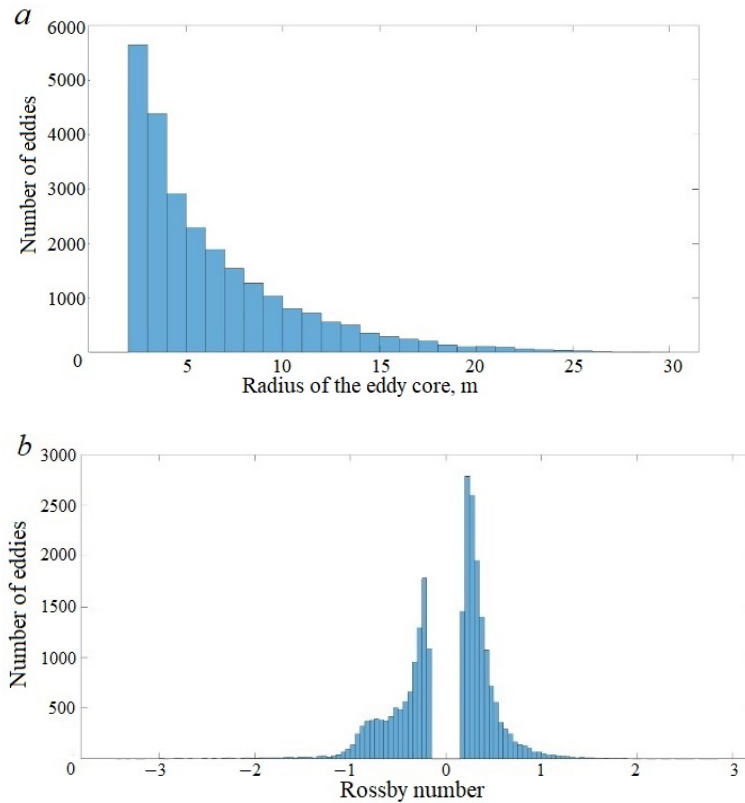


Fig. 2. Histograms of distribution of the core radius (*a*) and the Rossby number ($Ro = \zeta_{max}/f$) (*b*) of the identified eddies in the southeastern part of the Black Sea

From a dynamic view point, eddies that are in quasi-geostrophic balance can be considered mesoscale ($Ro \ll 1$, where Ro is the Rossby number equal to ζ/f ; ζ is the relative vorticity, and f is the planetary vorticity). In submesoscale dynamics, the Rossby number is on the order of unity, and the contribution of nonlinear terms in the equation of motion, which correspond to centrifugal acceleration (V^2/R), is comparable to the contribution of the Coriolis force ($V^2/R > fV$).

In this work, formations with $Ro > 0.5$ are classified as submesoscale eddies. The analysis showed that anticyclonic eddies (AE) were, on average, characterized by higher values of vorticity and Ro in their cores (Fig. 2, *b*). During the period under consideration, about 37% of the identified AEs and 17% of cyclonic eddies (CEs) had values of $Ro > 0.5$, i.e., they belonged to submesoscale ones. At the same time, about 5% of AE and 2% of CE had $Ro > 1$. Some eddies ($\sim 0.4\%$ AE and 0.01% CE) reached high Ro values (greater than 2.5).

It should be noted that most SCEs are located near large anticyclones and along the coastal zone. Fig. 3 shows the vorticity field distribution as of September 30, 2008. This example shows the accumulation of eddies on the outer and inner periphery of the BA, as well as the smaller Anatolian anticyclone located to the west of the BA. A large number of eddies is also observed near the eastern coast of the study area, in the coastal zone of high vorticity gradients.

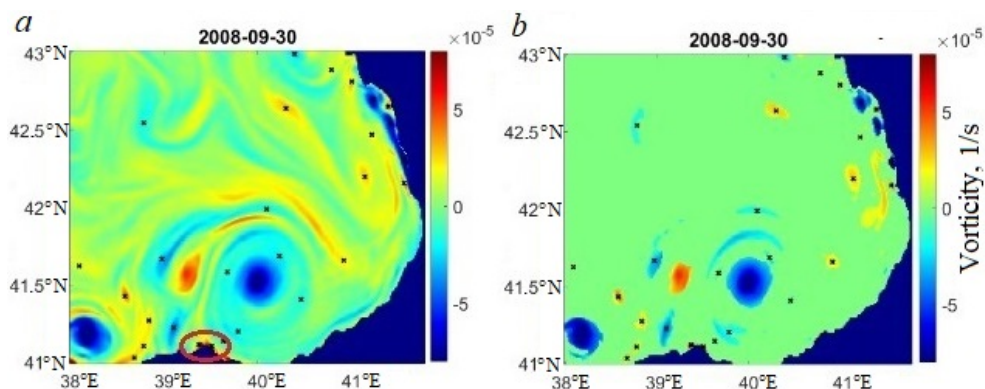


Fig. 3. Distribution of the vorticity field (*a*) and the selected areas in the vorticity field (*b*) based on the critical values of the OW parameter ($W > W_{kr}$) for 30.09.2008. Crosses mark the centers of the eddies whose radius is less than 10 km; red oval is Cape Fener

3.2. Formation of cyclonic eddies on the Batumi anticyclone periphery

During the study period, the longest-lived BA in the coastal zone of the study area was observed from the end of March 2008 to the middle of March 2009 (from 29.03.2008 to 16.03.2009). The BA was formed from the smaller Anatolian anticyclone, which at the beginning of April 2008 entered the study area from the west. By the end of April, its position had stabilized in the coastal zone at about 40°E east of the Turkish Cape Fener, marked in Fig. 3, *a* by a red oval. In the subsequent period, until the end of December 2008, the BA was located to the east of this cape, and after that time it began to move along the coast in the Black Sea Rim Current direction.

During the period of the BA presence in the coastal southeastern Black Sea, seven pronounced stable rounded SCEs were recorded on its periphery, which were formed at intervals of one week to two months: 04.08.2008, 19.09.2008, 16.11.2008, 02.12.2008, 11.12.2008, 10.02.2009. At the same time, in addition to stable SCEs, the formation of short-lived areas of high cyclonic vorticity, which have an elongated shape in the form of stripes, was much more often observed near the BA.

The analysis showed that most of the SCE is formed in the area of interaction between the BA waters and Cape Fener, located in its southwestern part (square in Fig. 4, *a*). A detailed process of generating one of these SCEs is shown in Fig. 4 (marked with red rectangles). It is clearly seen that when western currents go around the cape, a band of high cyclonic vorticity values formed at the BA periphery behind Cape Fener (Fig. 4, *a*). After a certain time, a pronounced cyclonic eddy with a radius of about 7 km is formed from this area (Fig. 4, *b – c*).

Thus, an important reason for the SCE generation was the interaction of BA waters, having high orbital velocities, with a topographic obstacle, the cape. Behind this cape, SCEs formed, then it separate from the shore, involved in the BA orbital motion and moved along its periphery to the north. Similar processes of SCE formation behind capes on the periphery of anticyclones near the coast of Crimea were observed in [4, 6] according to satellite data and drone measurements.

The formation of such SCEs occurred with some periodicity. To study the causes of SCE generation, the variability of the meridional velocity v and its shear $\frac{\partial v}{\partial x}$ on the zonal section passing from Cape Fener to the east was analyzed. The spatio-temporal diagram of this variability is shown in Fig. 5, *a*, *b*, and black lines in Fig. 5 show the moments of SCE formation at the cape. The SCE generation occurred after a period of an increase in the BA orbital velocity v and its approach directly to the cape (Fig. 5, *c*). The velocity increase in the coastal part causes an increase in shear directly near the coast in the coastal cells of the model (Fig. 5, *d*).

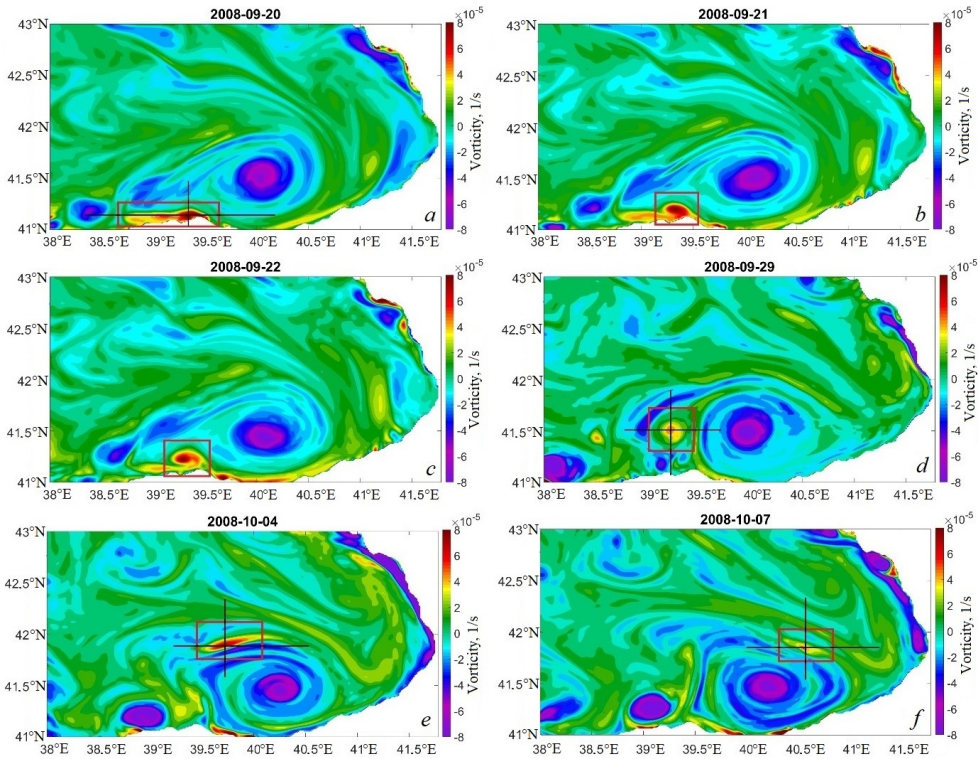


Fig. 4. Distributions of the current velocity vorticity on September, 20 (*a*); September, 21 (*b*); September, 22 (*c*); September, 29 (*d*); October, 4 (*e*) and October, 7 (*f*), 2008. The eddy is denoted by a red rectangle, the section location – by a cross

Following the pressing of the jet to the shore, the diagram (Fig. 5) shows a region of negative velocities v , i.e., a countercurrent directed to the south. Fig. 5, *b* demonstrates that at this moment a cyclonic vorticity zone $\frac{\partial v}{\partial x} < 0$ is formed near the cape. In this case, the cyclonic shear value reaches $(5-10) \cdot 10^{-5}$ 1/s, i.e. 0.5–1*f*. Such a shear leads to a sharp rise in isopycnal surfaces and an increase in the available potential energy of waters. The generation of attached cyclones was observed at the initial moment of the velocity shear increase. An exception to this regularity is the peak on October 1, 2008, when no eddy formation was observed.

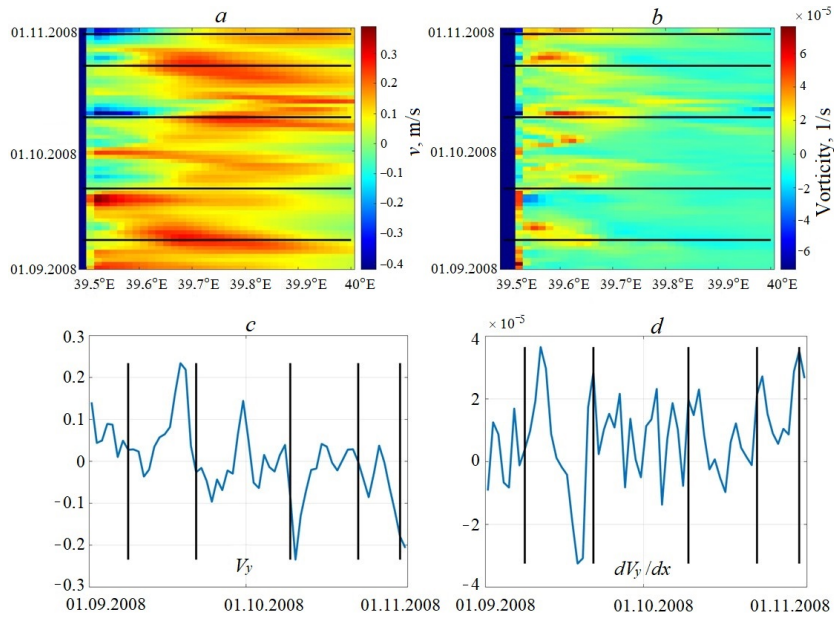


Fig. 5. Spatial-temporal diagram of meridional velocity v (*a*) and gradient $\frac{\partial v}{\partial x}$ (*b*) at the zonal section across Cape Fener at the 20 m depth for 01.09.2008–01.11.2008; variability of mean values v (*c*) and $\frac{\partial v}{\partial x}$ (*d*) at three points of the section which are the closest to the cape (at a distance 1–3 km). Black lines show the moments of forming the submesoscale eddies identified by visual analysis

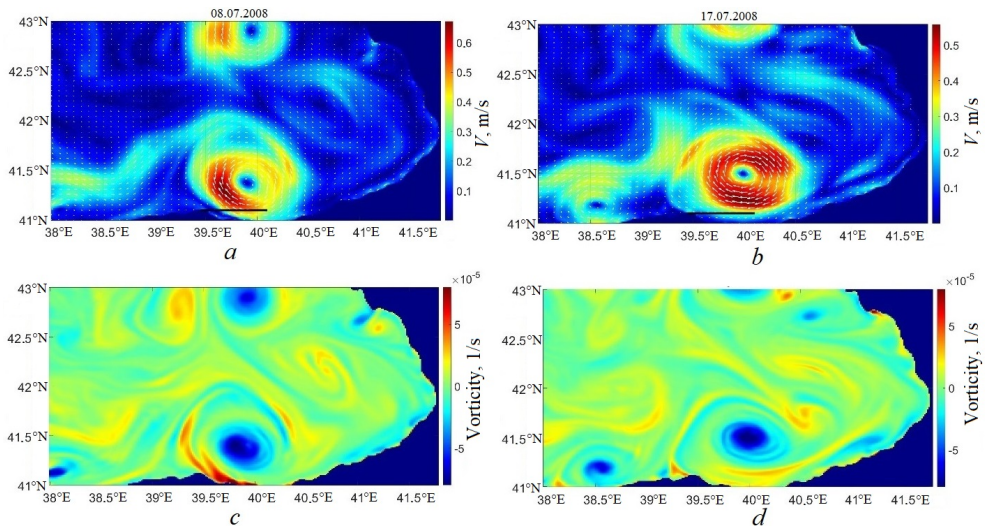


Fig. 6. Maps of the currents' velocity (*a*, *b*) and vorticity (*c*, *d*) at the 10 m horizon for July 8, 2008 (*a*, *c*) and July 17, 2008 (*b*, *d*) demonstrating an increase in cyclonic vorticity at the BA western periphery when it is pressed to the coast (*a*, *c*) and its decrease when the BA moves off the coast (*c*, *d*). Black line indicates the section position (see Fig. 5)

One of the reasons for the increase/decrease in the velocity of currents near the cape is the BA movement. In the course of its evolution, the BA moved along a cyclonic trajectory, periodically pressing against the coast or moving away from it (Fig. 6). Thus, on 08.07.2008 (Fig. 6, *a*), the BA center was located to the west of 40°E and the highest BA velocities were observed at a distance of less than 10 km from the cape. At the same time (Fig. 6, *c*), a band of cyclonic vorticity was observed to the BA southwest, which could subsequently transform into SCE (see Fig. 4). A few days later, on 17.07.2008 (Fig. 6, *b*), the BA shifted to the east, its center was located to the west of 40°N, and the distance from the cape to the maximum orbital velocity was 20–30 km. At the same time, the cyclonic vorticity areas (Fig. 6, *d*) were located relatively evenly around the BA, their values were much lower, and the attached SCEs were not formed.

It should be noted that the BA orbital velocity inhomogeneity can also be the cause of the velocity pulsation near the shore. In Fig. 6, *a*, it is noticeable that the BA orbital velocity in its western part was much higher than in the eastern one.

3.3. Development of attached submesoscale cyclones on the example of an eddy in September – October, 2008

Let us consider the SCE evolution on the example of an eddy formed in September, 2008 (hereinafter referred to as C1). Here, the eddy tracking was carried out using the developed algorithm. The considered eddy trajectory is plotted on the vorticity field of the currents at the time of the last fixation of the C1 eddy (Fig. 7). As can be seen, the C1 eddy moved along the eddy periphery along an anticyclonic trajectory. The eddy existed for 20 days and covered a distance of about 220 km during this period.

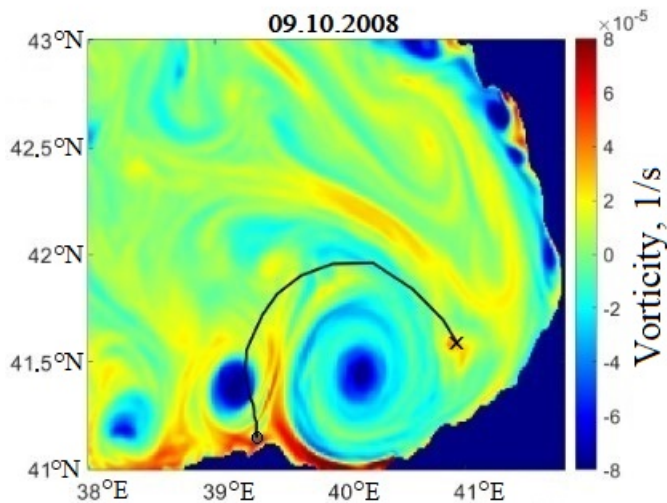


Fig. 7. Trajectory of one of the attached SCEs. Circle indicates the place of its first identification (19.09.2008), and cross – position at the last moment of its identification (9.10.2008). Color scale shows distribution of the current velocity field vorticity at the 20 m depth on 09.10.2008

The detailed evolution of this eddy in the vorticity field is shown in Fig. 4. The C1 eddy was formed on September 19 after the passage of a part of the BA with a maximum orbital velocity in the coastal zone of Cape Fener. At the moment shown in Fig. 7, the eddy does not have a clear local structure. It is located in a narrow (about 10 km wide) band of high vorticity values extended along the coast for a distance of approximately 90–100 km (see Fig. 4, *a*).

Having formed behind the cape, the eddy starts moving north. Then, on September 23, a strip with high vorticity values broke away from the coast and a round cyclone with a radius of 15 km was formed from it (see Fig. 4, *b, c*). Further, from September 23 to September 30, the C1 eddy, entrained by the BA waters with an orbital speed of ~ 0.5 m/s, moves anticyclonically to the northern part of the BA with an average speed of 0.05 m/s. On the 10th day of its existence (29.09.2008), the C1 eddy is well defined and looks like a round spot of increased vorticity about 20 km in diameter (see Fig. 4, *d*). The orbital velocity of C1 is 0.2 m/s.

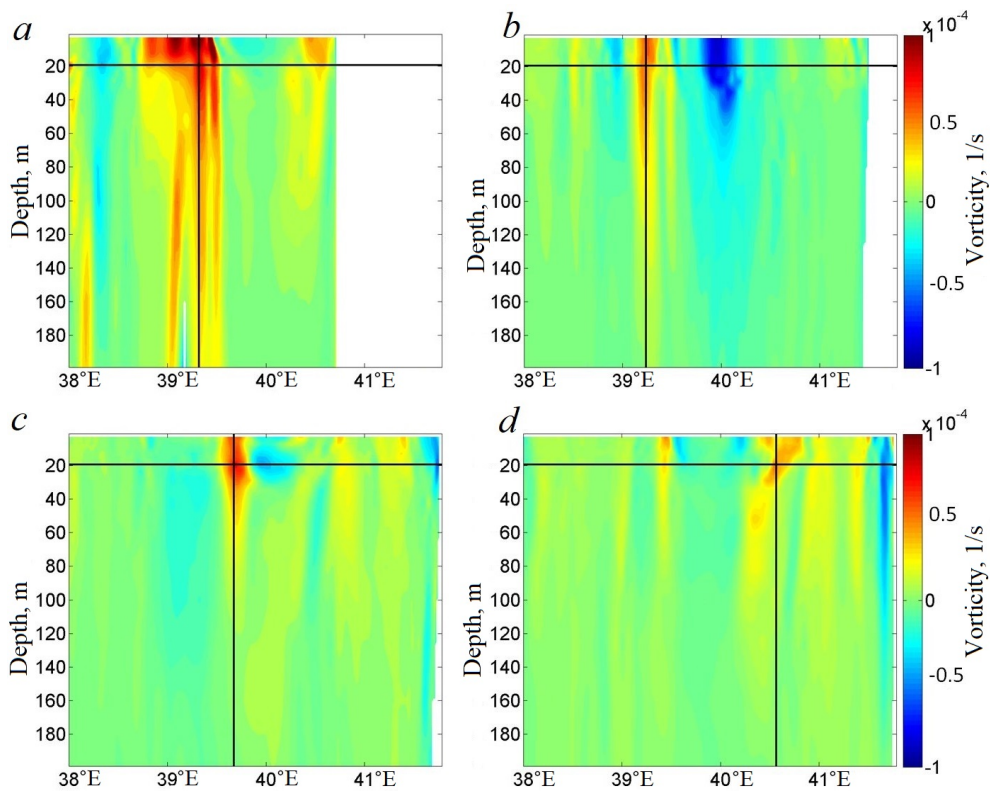


Fig. 8. Vorticity meridional sections through the eddy center for September, 20 (*a*), September, 29 (*b*), October, 4 (*c*) and October, 7 (*d*), 2008 (see Fig. 4)

A vertical section through the C1 eddy center at its formation time (20.09.2008), presented in Fig. 8, *a*, shows that the formed eddy occupies a large water column and causes a significant increase in vorticity in the 0–200 m layer. In the upper 0–20

m layer, its diameter is about 25 km, below the horizon 20 m – $\sim 10\text{--}15$ km. The vorticity in the attached SCE reaches high values (up to $1.2 \cdot 10^{-4}$ 1/s), which are comparable to the vorticity values in the BA center in the 0–50 m layer (Fig. 8, *b*). At greater depths, the C1 eddy vorticity exceeds the BA vorticity by several times. In the same 0–200 m layer, a sharp increase in the vertical velocity value is observed (Fig. 9, *c, d*). Thus, the attached SCEs (Fig. 8) cause significant changes in the dynamic structure of waters in deep layers. These changes are much more significant than in the parent BA. The values of vertical velocities (Fig. 9, *c*) exceed 10^{-4} m/s, i.e., they are more than 10 m/day, which is an order of magnitude greater than in the BA.

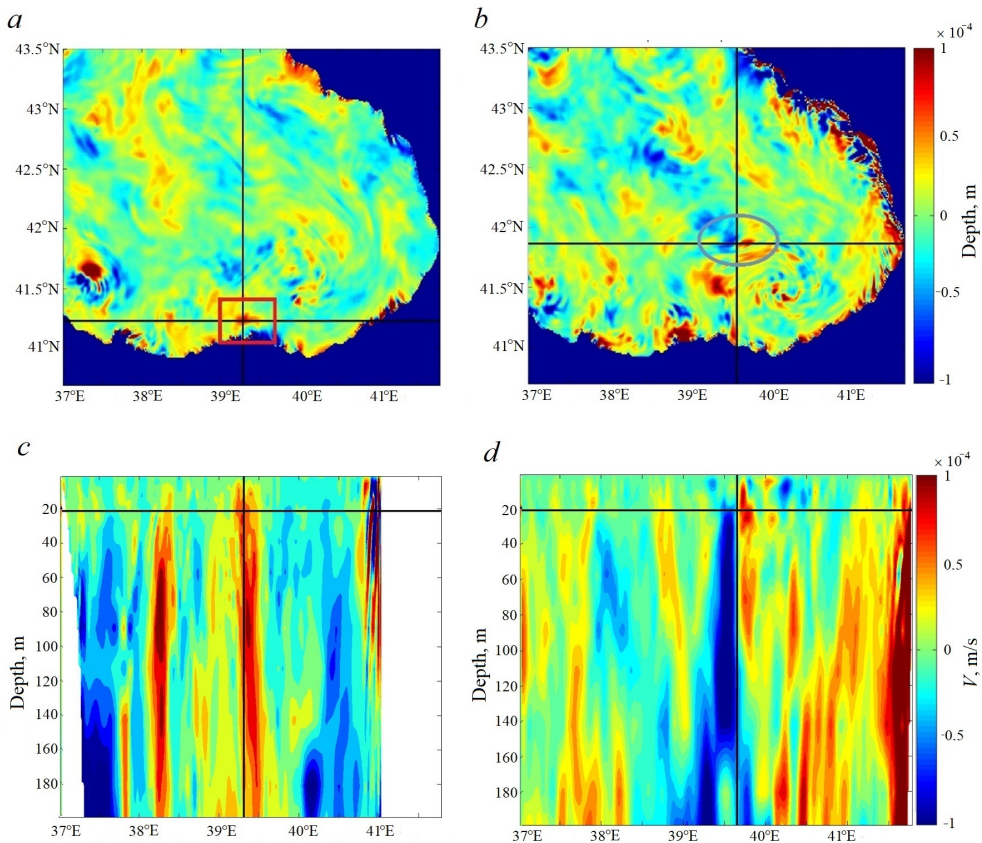


Fig. 9. Distribution of vertical velocities at the 20 m depth (*a, b*) and their sections through the eddy center C1 (*c, d*) during its intensification (September 21, 2008) (*a, c*) and weakening (October 04, 2008) (*b, d*)

Such large vertical velocities significantly affect the thermohaline structure of waters. Fig. 10 shows maps of temperature and salinity at a depth of 20 m for September 29. The C1 eddy is clearly distinguished as a round cold spot (Fig. 10, *a*) at the warm BA periphery. The temperature at a depth of 20 m is about 12°C , which is $\sim 10^{\circ}\text{C}$ lower than in the BA (24°C). The vertical temperature section

shows that the seasonal thermocline is elevated in the SCE region (Fig. 10, *c*). As a result of intense mixing in the upper layer of 0–20 m, the temperature in the C1 eddy is 4 °C lower than in the surrounding waters.

The salinity map clearly shows a sharp positive anomaly in the CE core, surrounded by fresher waters detached from the BA (Fig. 10, *b*). The salinity in the CE center is 18.2, which is 0.2 higher than in the surrounding waters and 0.4 higher than in the downwelling area in the BA. The positive anomaly of salinity in Fig. 10, *d* is noticeable in the upper 25 m layer. At the same time, the increased salinity area is wider than the low temperature one, which is probably due to the more conservative character of salinity changes. The analysis shows that the cold and salt anomalies were formed in the initial period of eddy generation, after which they gradually weaken.

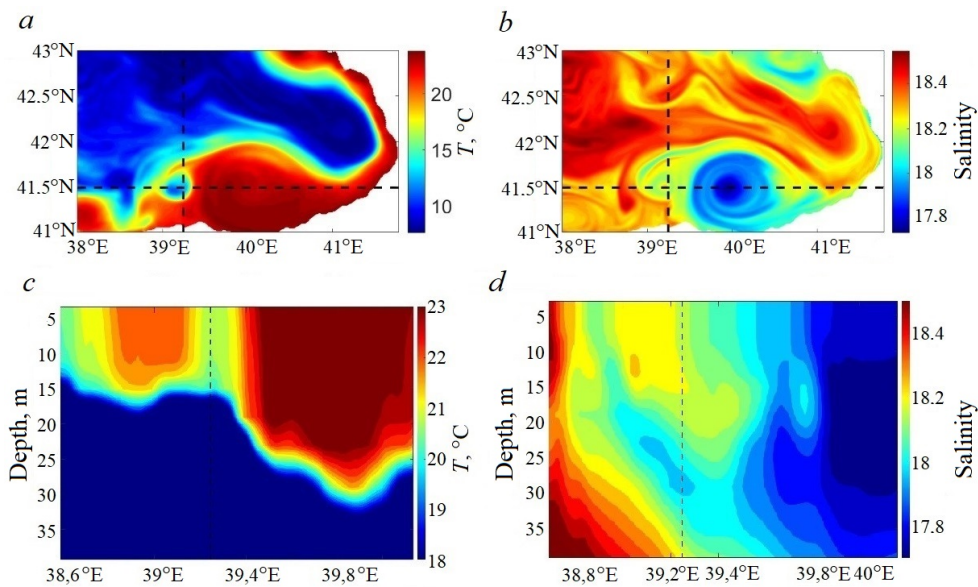


Fig. 10. Distribution of temperature (*a*) and salinity (*b*) at the 20 m depth for September 29, 2008; the temperature (*c*) and salinity (*d*) sections through the eddy center C1 in the salinity field for 29.09.2008 and 7.10.2008

3.4. Dissipation of attached submesoscale cyclones on the C1 eddy example in September – October 2008

On September 30 (see Fig. 4, *e*), the C1 eddy begins to stretch along the BA perimeter. The stretching implies a rapid increase in the positive vorticity area along the BA perimeter. The map for October 4, 2008 clearly shows that the size of this region along the BA periphery grows to ~ 120 km, while the transverse dimensions decrease to 10 km.

During the eddy evolution, the radius of its core (the radius of the region of high OW parameter values) decreases from the maximum values of 12 km during its development to 3–7 km at the end of its existence (Fig. 11, *a*). At the same time, its

eccentricity grows from 0.4 to 0.9, i.e., the ratio of the major and minor semiaxes changes from 0.7 to 0.3 (Fig. 11, *b*). Thus, the initially rounded and rather large eddy is elongated, its core decreases in size and takes a strongly elliptical shape.

At this moment, the C1 eddy movement speed along the BA also increases significantly – six times (from 0.05 to 0.3 m/s) (Fig. 11, *c*). At the same time, the leading edge of the zone of high vorticity values as a result of stretching moves at a speed of 0.7 m/s, and the rear one – at a speed of 0.3 m/s, which corresponds to the speed of background currents at the BA periphery, ranging from 0.3 to 0.7 m/s (see Fig. 6, *a, b*). With the beginning of the eddy stretching process, on September 30, the vertical velocity structure (see Fig. 9, *c, d*) takes a dipole form: positive vertical velocities dominate at the leading edge of the cyclone, and negative ones – at the trailing edge.

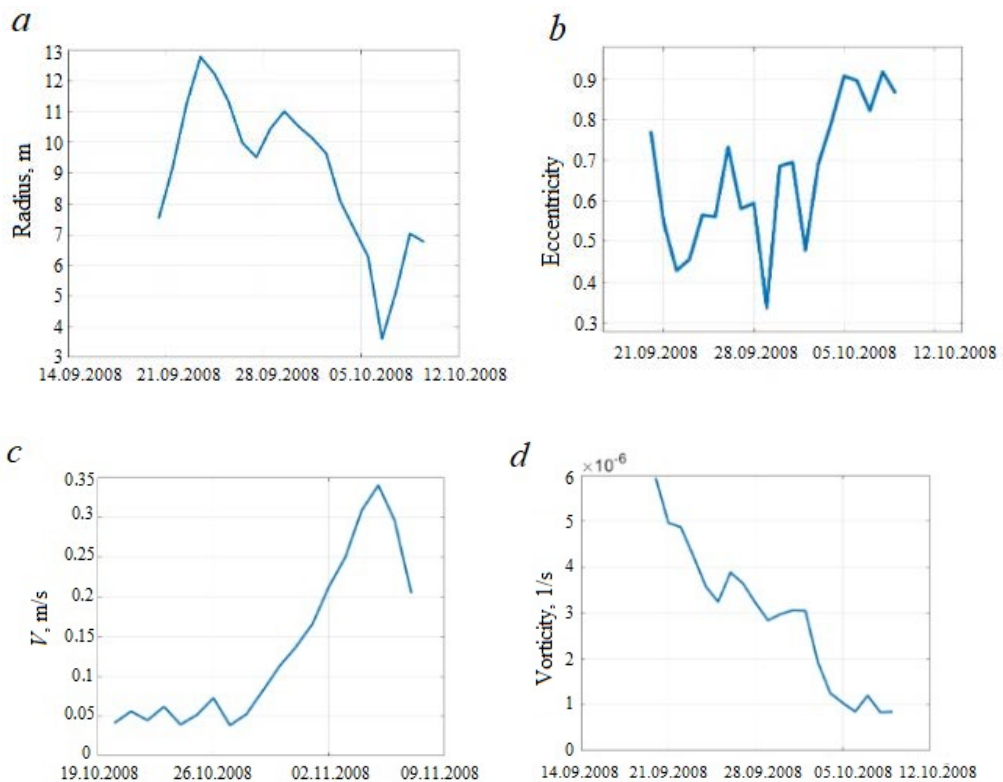


Fig. 11. Characteristics of the cyclone C1 in the process of its evolution in September 19 – October 9, 2008: *a* – the eddy equivalent radius; *b* – the eddy eccentricity; *c* – the movement velocity; *d* – the eddy average vorticity in the 0–100 m layer

The reason for the eddy stretching is probably a sharp horizontal velocity shear between the BA periphery and the surrounding waters. The velocity field analysis shows that the beginning of this process is observed in the BA velocity intensification zone. The velocity shear of the background currents leads to the fact

that the density anomalies on its southern periphery move east with a greater speed, and on the northern periphery – to the south.

The process of the eddy energy reducing during its elongation was considered in detail in [22]. It follows from the vorticity conservation law that the eddy volume and the product of its semi-axes must be kept constant. This process leads to the eddy stretching – a consistent increase in the area of the density anomaly zone and a decrease in the eddy thickness. This causes a decrease in the eddy speed and energy, which is proportional to the vertical density anomaly integral of the eddy. As a result, unlike September 29, on the 16th day of existence (04.10.2008), the region of high vorticity values ($\zeta > 5 \cdot 10^{-5}$) occupies not 200 m, but only the upper 40 m (see Fig. 8, *c*). On the 19th day of its existence, C1 reaches the BA northeastern periphery. It stretches even more along the BA periphery (see Fig. 4, *f*), turning into an eddy filament [22]. Fig. 8, *d* shows that C1 loses its slender structure, its axis tilts in the direction of motion, the vorticity significantly decreases and is observed only in the upper 20 m layer. This structure persists until the complete dissipation of the eddy, which occurs on October 10, 2008.

The author of [22] showed that stretching increases as the eddy weakens relative to the background current velocity. The graph of the mean vorticity in the 0–100 m layer (Fig. 11, *d*) shows that C1 has the highest vorticity ($\sim 6 \cdot 10^{-6}$ 1/s) at the moment of its generation. In the evolution process, its vorticity constantly decreases, decreasing by half in 10 days after the eddy formation. Thus, at the beginning of its formation, the eddy has the greatest nonlinearity, which decreases as it moves. This indicates that the potential energy of the eddy is primarily associated with the external force acting at the moment of its formation, when a sharp area of water rises behind the cape. After the eddy formation, the energy begins to slowly dissipate, the eddy weakens. It results in the decrease of its resistance to tension [22]. The stretching speed of the elongated eddy increases, which leads to its complete dissipation and transformation into the eddy filament.

Conclusions

In the present paper, based on high-resolution numerical model calculations, a detailed study of the development, evolution and dissipation of submesoscale cyclones at the BA periphery is carried out. The results show the following:

1. SCEs are formed during the Batumi anticyclone intensification and its displacement to the west towards Cape Fener. As a result of an increase in velocity shear during the interaction of the Batumi anticyclone waters with the cape, a positive vorticity area is formed, which in some cases transforms into SCE. This SCE then separates from the coast and moves along the BA periphery in the anticyclonic direction. At the moment of its formation, the eddy is characterized by the highest vorticity, energy, salinity and temperature anomalies. Some SCEs are able to exist for more than 20 days and move over a distance of more than 100 km, reaching the northeastern BA periphery, which is also confirmed by satellite measurements.

2. The analysis of the SCE vertical structure shows that they occupy a large water column, reaching a depth of 200 m. At the same time, the vorticity values in

them can be up to $1 f$, and the vertical velocity in the entire 0–200 m layer can be more than 10 m/day. Thus, SCEs have a significant local effect on the vertical structure and dynamic characteristics of the waters of the entire upper 200 m layer. Their influence is well manifested in the fields of temperature and salinity, since these eddies cause the rise of cold salty waters.

3. The SCE dissipation is related to their stretching along the direction of motion. Stretching is initiated by a significant velocity shift at the parent anticyclone periphery. The stretching process begins in the middle of the eddy lifetime after its weakening. The shear leads to an expansion of the area of the increased density anomaly and the decrease of its thickness, which causes further SCE weakening. The subsequent eddy stretching leads to its complete dissipation and transformation into an elongated zone of positive vorticity – a vortex line.

REFERENCES

1. McWilliams, J.C., 2016. Submesoscale Currents in the Ocean. *Proceedings of the Royal Society A: Mathematical, Physical and Engineering Sciences*, 472(2189), 20160117. doi:10.1098/rspa.2016.0117
2. Korotaev, G.K. and Shutyaev, V.P., 2020. Numerical Simulation of Ocean Circulation with Ultrahigh Spatial Resolution. *Izvestiya, Atmospheric and Oceanic Physics*, 56(3), pp. 289-299. doi:10.1134/S000143382003010X
3. Stanev, E.V., Ricker, M., Grayek, S., Jacob, B., Haid, V. and Staneva, J., 2020. Numerical Eddy-Resolving Modeling of the Ocean: Mesoscale and Sub-Mesoscale Example. *Physical Oceanography*, 27(6), pp. 631-658. doi:10.22449/1573-160X-2020-6-631-658
4. Puzina, O.S., Kubryakov, A.A. and Mizyuk, A.I., 2021. Seasonal and Vertical Variability of Currents Energy in the Sub-Mesoscale Range on the Black Sea Shelf and Its Central Part. *Physical Oceanography*, 28(1), pp. 37-51. doi:10.22449/1573-160X-2021-1-37-51
5. Kubryakov, A.A., Lishaev, P.N., Cheryzhenko, A.I., Aleskerova, A.A., Kubryakova, E.A., Medvedeva, A.V. and Stanichny, S.V., 2021. Impact of Submesoscale Eddies on the Transport of Suspended Matter in the Coastal Zone of Crimea Based on Drone, Satellite, and in Situ Measurement Data. *Oceanology*, 61(2), pp. 159-172. doi:10.1134/S0001437021020107
6. Aleskerova, A., Kubryakov, A., Stanichny, S., Medvedeva, A., Plotnikov, E., Mizyuk, A. and Verzhvskaya, L., 2021. Characteristics of Topographic Submesoscale Eddies off the Crimea Coast from High-Resolution Satellite Optical Measurements. *Ocean Dynamics*, 71(6–7), pp. 655-677. <https://doi.org/10.1007/s10236-021-01458-9>
7. Mahadevan, A., 2016. The Impact of Submesoscale Physics on Primary Productivity of Plankton. *Annual Review of Marine Science*, 8, pp. 161-184. <https://doi.org/10.1146/annurev-marine-010814-015912>
8. Mikaelyan, A.S., Zatsepin, A.G. and Kubryakov, A.A., 2020. Effect of Mesoscale Eddy Dynamics on Bioproductivity of the Marine Ecosystems (Review). *Physical Oceanography*, 27(6), pp. 590-618. doi:10.22449/1573-160X-2020-6-590-618
9. Demyshev, S.G. and Evstigneeva, N.A., 2016. Modeling Meso- and Sub-Mesoscale Circulation along the Eastern Crimean Coast Using Numerical Calculations. *Izvestiya, Atmospheric and Oceanic Physics*, 52(5), pp. 560-569. doi:10.1134/S0001433816050042
10. Zatsepin, A.G., Baranov, V.I., Kondrashov, A.A., Korzh, A.O., Kremenetskiy, V.V., Ostrovskii, A.G. and Soloviev, D.M., 2011. Submesoscale Eddies at the Caucasus Black Sea Shelf and the Mechanisms of Their Generation. *Oceanology*, 51(4), 554. doi:10.1134/S0001437011040205
11. Zatsepin, A., Kubryakov, A., Aleskerova, A., Elkin, D. and Kukleva, O., 2019. Physical Mechanisms of Submesoscale Eddies Generation: Evidences from Laboratory Modeling and

- Satellite Data in the Black Sea. *Ocean Dynamics*, 69(2), pp. 253-266. doi:10.1007/s10236-018-1239-4
12. Brannigan, L., 2016. Intense Submesoscale Upwelling in Anticyclonic Eddies. *Geophysical Research Letters*, 43(7), pp. 3360-3369. <https://doi.org/10.1002/2016GL067926>
 13. Brannigan, L., Marshall, D.P., Naveira Garabato, A.C., George Nurser, A.J. and Kaiser, J., 2017. Submesoscale Instabilities in Mesoscale Eddies. *Journal of Physical Oceanography*, 47(12), pp. 3061-3085. doi:10.1175/JPO-D-16-0178.1
 14. Ivanov, V.A. and Belokopytov, V.N., 2013. *Oceanography of the Black Sea*. Sevastopol: MHI, 210 p.
 15. Kubryakov, A.A. and Stanichny, S.V., 2015. Dynamics of Batumi Anticyclone from the Satellite Measurements. *Physical Oceanography*, (2), pp. 59-68. doi:10.22449/1573-160X-2015-2-59-68
 16. Kubryakov, A.A. and Stanichny, S.V., 2015. Mesoscale Eddies in the Black Sea from Satellite Altimetry Data. *Oceanology*, 55(1), pp. 56-67. doi:10.1134/S0001437015010105
 17. Madec, G. and the NEMO team, 2016. *NEMO Ocean Engine*. Note du Pôle de modélisation de l'Institut Pierre-Simon Laplace No 27. 386 p. [online] Available at: <http://www.nemo-ocean.eu/doc/> [Accessed: 10 September 2019].
 18. Mizyuk, A.I., Korotaev, G.K., Grigoriev, A.V., Puzina, O.S. and Lishaev, P.N., 2019. Long-Term Variability of Thermohaline Characteristics of the Azov Sea Based on the Numerical Eddy-Resolving Model. *Physical Oceanography*, 26(5), pp. 438-450. doi:10.22449/1573-160X-2019-5-438-450
 19. Mizyuk, A.I. and Korotaev, G.K., 2020. Black Sea Intrapycnocline Lenses According to the Results of a Numerical Simulation of Basin Circulation. *Izvestiya, Atmospheric and Oceanic Physics*, 56(1), pp. 92-100. doi:10.1134/S0001433820010107
 20. Weiss, J., 1991. The Dynamics of Enstrophy Transfer in Two-Dimensional Hydrodynamics. *Physica D: Nonlinear Phenomena*, 48(2-3), pp. 273-294. [https://doi.org/10.1016/0167-2789\(91\)90088-Q](https://doi.org/10.1016/0167-2789(91)90088-Q)
 21. Belonenko, T.V. and Sholeninova, P.V., 2016. On Identification of Mesoscale Eddies from Satellite Altimetry Based on the Area in the NW Pacific. *Sovremennye Problemy Distantionnogo Zondirovaniya Zemli iz Kosmosa*, 13(5), pp. 79-90. doi:10.21046/2070-7401-2016-13-5-79-90 (in Russian).
 22. Zhmur, V.V., 2010. *Mesoscale Ocean Eddies*. Moscow: GEOS, 290 p. (in Russian).

About the authors:

Artyom A. Bogdanov, Senior Research Engineer, Marine Hydrophysical Institute of RAS (2 Kapitanskaya St., Sevastopol, 299011, Russian Federation), **ORCID ID: 0000-0001-9890-3854**, artem96.96@bk.ru

Arseniy A. Kubryakov, Senior Research Associate, Marine Hydrophysical Institute of RAS (2 Kapitanskaya St., Sevastopol, 299011, Russian Federation), Ph.D. (Phys.-Math), **ORCID ID: 0000-0003-3561-5913**, arskubr@mhi-ras.ru

Artyom I. Mizyuk, Senior Research Associate, Marine Hydrophysical Institute of RAS (2 Kapitanskaya St., Sevastopol, 299011, Russian Federation), Ph.D. (Phys.-Math), **ORCID ID: 0000-0003-4885-354X**, **ResearchID: C-6125-2016**, artem.mizyuk@mhi-ras.ru

Contribution of the co-authors:

Artyom A. Bogdanov – data analysis, visualization, formulation of results and preparation of the final version of the paper text

Arseniy A. Kubryakov – numerical calculations, preparation of the paper text

Artyom I. Mizyuk – setting tasks, choosing research methods, preparation of the paper text

The authors have read and approved the final manuscript.

The authors declare that they have no conflict of interest.